A mathematical examination of the impact of mould transparency to infrared radiation on solidification during the investment casting process

C A Jones[1], A E W Jarfors[2], E Rogers[3], P Vrethed[4], P Silva[4], M R Jolly[1]

[1] Sustainable Manufacturing System Centre, School of Aerospace, Transport and Manufacturing, Cranfield University, Bedfordshire, MK43 0AL, UK
[2] Jönköping University, School of Engineering, Box 1026, 551 11 Jönköping, Sweden
[3] Surface Engineering and Precision Centre, School of Aerospace, Transport and Manufacturing, Cranfield University, Bedfordshire, MK43 0AL
[4]TPC Components AB, Brånstaleden 2, 734 32 Hallstahammer, Sweden

Email: c.a.jones@cranfield.ac.uk

Abstract. Investment casting is a highly dynamic process during which multiple competing physical phenomena are at work. Those seeking to understand and simulate such processes computationally are confronted with a considerable task, balancing accuracy with efficiency. Approximations and models based on well-understood and documented fundamental physics are powerful tools in a modeller's arsenal. Driven by observed discrepancies between experimental thermocouple measurements and simulation predictions of casting temperatures, this work explores the additional alloy cooling mechanism of mould transparency to infrared radiation, targeting a new mathematical approximation applicable in such situations. Direct attenuation, scattering from coarse sand, sand distribution in the mould and material temperatures play a role in the extent of radiation transparency that must be considered. From this model, estimation of the additional cooling rate resulting from expected mould transparency can be determined and applied as a corrective measure to computation fluid dynamics (CFD) simulation results that do not capture this phenomenon.

1. Introduction

Managing heat transfer in any casting process is crucial in controlling the generation of many casting defects such as misruns, undesirable microstructures and residual stresses [1]. Such defects are particularly prolific when producing aerospace turbine blades via investment casting where the component's large area, thin cross-sectional regions are a principal source of such issues. Management of these thermal flows is generally controlled by applying insulating wool fibre to the mould which prevents excessive heat loss, alternatively through increasing mould porosity or adjusting mould composition to improve the overall insulating capability of the mould. These solutions are admirable at controlling heat transfer by thermal conductivity, and in general for radiation heat transfer but rely on radiation interacting with the mould. Previous research conducted into understanding and validating the thermophysical properties of an investment casting mould [2] succeeded, in addition to those aims, in identifying an alloy cooling in experimentation greater than that predicted using CFD simulations. This suggests that a quantity of thermal energy escaping from the casting, in reality, has been omitted from heat transfer consideration within the simulation calculations. It is hypothesised that the relatively high porosity, Silica based investment casting mould used in the manufacture of Nickel-based superalloys could result in a mould system with non-negligible transparency to infrared radiation leading to an

additional, uncontrolled cooling of the alloy. It is this hypothesis that this work seeks to investigate through discussion of the interaction between electromagnetic (EM) radiation and matter in comparison to experimental transmission measurements conducted on the mould material.

2. Theoretical Model

EM radiation passing through solid matter has a common mathematical root defined by Maxwell's equations and applies irrespective of the solid material properties or composition (although such details are required for a solution). As such, this represents an admirable starting point for constructing a generic, mathematical description of radiation semi-transparency. It is common knowledge that EM radiation consists of a combination of orthogonal electric and magnetic fields, but the magnetic component is generally negligible compared to the electric field element during interactions with matter [3]. Equation 1 shows the expanded form of such an electric field of an arbitrary EM wave based on Maxwell's equations that describes the electric field strength at a position, x, within a material at a time, t. This expansion is based on a substitution for the velocity, v, in terms of the complex refractive index, ${}^{1}/_{v} = {}^{n}/_{c} - {}^{ik}/_{c}$. Here n is the real portion and k is the imaginary part of the complex refractive index with c representing the velocity of light.

$$E = E_0 e^{i2\pi f[t-({}^{x}/_{v})]} \rightarrow E = E_0 e^{(i2\pi ft)} e^{-\left({}^{i2\pi xn}/_{c}\right)} e^{-\left({}^{2\pi fkx}/_{c}\right)}$$

Equation 1. Mathematical wave equation for the electric field component of a generic electromagnetic wave propagating through a solid.

Developing this theory, let us consider the associated power of an EM wave which can be defined by the square of the electric field strength multiplied by the electrical conductivity of the solid, σ_e. Taking the ratio between the power at a generic position, x, in the material and the initial power, as shown in Equation 2, reduces the expression considerably to a single exponential governing the damping of radiation passing through a material. The exponent of this exponential can be expressed in terms of either frequency, f, or wavelength, λ_w, and are related through the velocity of light, $f = {}^{c}/_{\lambda_w}$.

$$\frac{P(x)}{P(0)} = \frac{\sigma_e E(x)^2}{\sigma_e E(0)^2} = e^{-\left({}^{4\pi fkx}/_{c}\right)} = e^{-\left({}^{4\pi kx}/_{\lambda_w}\right)} = e^{-\alpha x}$$

Equation 2. The ratio of the EM wave power at position x to the initial EM wave power at position zero

The salient result of these equations is the definition of the absorption coefficient, α, from this remaining exponential which introduces the material specifics into the problem through the extinction coefficient, k (imaginary part of the complex refractive index). This wavelength-dependent parameter governs the attenuation per metre as EM radiation passes through a material. The wavelength-dependent makes sense as it would not be expected that materials would respond similarly when exposed to different radiation sources. Absorption in different atomic structures and atoms would give rise to variance in the extinction coefficients for composite solids.

Developing this equation further, the subject of the formula can be translated analogously into radiation intensity in terms of the absorption coefficient – a far more practical form as shown in Equation 3. It should be made clear that the same exponential term derived previously appears in this expression but here as a one minus value (bracketed term). This is an essential alteration as this allows the expression to predict the intensity of radiation at position x that survives to propagate further into the solid.

$$I = I_0(1 - e^{-\alpha x}) = \varepsilon_a \sigma T^4 (1 - e^{-\alpha x})$$

Equation 3. Electromagnetic wave intensity that successfully penetrates a distance x into a material. Valid for a uniform composition material.

The initial intensity of the incident radiation, I_0, has been elaborated on by considering the emitting radiation source. It can be assumed that any hot object will emit energy as a blackbody. The Stefan-Boltzmann law [3] defines the emission intensity based on the fourth power of the emitter's surface temperature and the Stefan-Boltzmann constant, σ. The alloy emissivity, ε_a, is also a consideration as no object truly emits as a perfect radiator; an emission inefficiency must be considered. A study of the

blackbody spectrum provides a second piece of essential information to introduce; the wavelength at which the radiation will be emitted depending on the source temperature, which is required for absorption coefficient calculation. The peak of a blackbody spectrum defines the most probable wavelength of emission dependent on the surface temperature, which changes inversely with temperature following Wein's displacement law [3], Equation 4.

$$\lambda_w = \frac{2.898 \times 10^{-3}}{T}$$

Equation 4. Wien's displacement law for calculation of the most probable wavelength of emission from an object based on surface temperature in Kelvin

Equation 3 represents the most basic understanding of the attenuation of EM radiation during interaction with matter, as it only considers a single homogeneous material. Setting the value of x to the corresponding total thickness of a casting mould would grant a basic transmittance estimate for a single composition, homogeneous material. For more realistic composite materials, there will be multiple absorption coefficients to consider, addressed by multiplying the corresponding thickness of each absorber with the absorption coefficient and summing the results in the exponent. Considering that emission will occur from all surfaces of the casting, and because the mould completely encases the casting, it can be assumed that radiation emitted from the casting will pass through the mould system without exception. Hence the volume fraction of each material can be used in place of the corresponding material thickness that an incident beam would encounter. Generally, this is easier to determine compared with physical distances and has the major advantage of independence from the angle of incidence, so it will not be impacted by scattering angles and boundary reflection phenomena.
It is not only direct attenuation that affects the passage of radiation in solids, but also surface reflections and scattering interactions with large particulates and defects. Firstly, because investment casting moulds are constructed layered, escaping radiation must cross each interface irrespective of the surface emission point. Should the successive layers have significant differences in refractive index, reflections will occur that will reduce the intensity of the propagating radiation as per Equation 5 [4]. The calculated reflectance, ranging between 0 and 1, would appear in mathematics as a multiplicative factor that reduces the initial intensity.

$$R = \left(\frac{n_1 - n_2}{n_1 + n_2}\right)^2$$

Equation 5. Surface reflectance in terms of the refractive index of medium 1, n_1, and medium 2, n_1

Scattering is a complex phenomenon dependent on multiple factors that must be considered on a case-by-case basis. Scattering behaviour depends on the relative disparity between the particle size (d) and the radiation wavelength interacting with them. Broadly, scattering can be segregated into three regimes; Rayleigh ($d \ll \lambda_w$), Mie ($d \sim \lambda_w$) and Optical ($d \gg \lambda_w$) scattering [5]. In investment casting, even the fine stucco particles present in the mould prime coat (90 mesh) will generally be several orders of magnitude larger than the radiation wavelength. As such, scattering behaviour in these systems will be driven by optical scattering descriptions. Several models for optical scattering can be relevant when the underlying assumptions are in line with the facts of the casting system. Arguably more helpful than an assumed model are phase functions, which are probability distributions defining the angular distribution of intensity around a particle following a scattering event. An example of such a phase function employed in this model is the Henyey-Greenstein (HG) phase function [6], detailed in Equation 6, which can be applied to particles of nanometres to millimetres scales. The parameter g is known as the anisotropy factor spanning the range zero to one and is used to tune the angular distribution to a specific system. Depending on the selection, the intensity distribution can be altered from uniform scattering ($g = 0$), to preferentially backwards ($g < 0$) or forwards ($g > 0$) scattering. This parameter is not selected arbitrarily but instead calculated from the cosine expectation value, $g = \langle cos(\theta) \rangle$ [7].

$$P(g,\theta) = \frac{1}{4\pi}\frac{(1-g^2)}{[1+g^2-2g\,cos(\theta)]^{3/2}}$$

Equation 6. Henyey-Greenstein (HG) phase function in terms of scattering angle, θ, and anisotropy factor, g

This phase function can be integrated before unification with the wider theory which, although not essential, reduces future calculations. Defining interest as the quantity of intensity that is not able to escape from the solid, the upper and lower integration limits can be set at π and $\pi/2$ respectively. Equation 7 shows the results of performing this integration by substitution ($\mu = cos(\theta)$), where the additional factor of 2π is included for normalisation. The result of this integration, the backscatter fraction ($S_{BS}(g)$) ranges from zero to one and now depends solely on the anisotropy factor as the angle has been integrated out through defined limits.

$$S_{BS}(g) = 2\pi\int_{\pi/2}^{\pi}\frac{1}{4\pi}\frac{(1-g^2)}{[1+g^2-2g\,cos(\theta)]^{3/2}}d\theta = \int_0^{-1}\frac{1}{2}\frac{(1-g^2)}{[1+g^2-2g\mu]^{3/2}}d\mu$$

$$S_{BS}(g) = \frac{1-g}{2g}\left(\frac{g+1}{\sqrt{g^2+1}}-1\right)$$

Equation 7. Fraction of backscattered intensity calculated from the integration of the HG function via substitution method

This simplified expression can be used directly in the theoretical model as a multiplicative factor acting to reduce the outbound intensity. In systems with a low concentration of scattering elements, the backscatter fraction can be scaled by the ratio of the total scattering cross-section to the emitting surface area, equivalent to the volume fraction. As with the boundary reflections, this backscatter fraction will appear one minus the value in the final expression as it is the fraction of escaping radiation sought. The backscatter angle was chosen for the integration to allow consideration of an effective thermal conductivity parameter in future work. Integration has a secondary importance; literature suggests estimation of backscattering using the HG function specifying both g and θ gives poor results [6]. Integrating across a range of angles improves accuracy by broadening the field of interest. Using the HG function without integration remains possible through an alternative form, the double HG function [6], which consists of summing two weighted HG functions where one has a positive anisotropy factor and the second has a negative anisotropy factor. The weighting represents the relevant dominance of the associated forward and backscattering. Given that the integrated single HG function reports satisfactory values when considering backscattering, the choice was made to use this simpler variant in the final expression over the more complex double function that has the potential to introduce additional uncertainty through a second anisotropy factor and weightings.
Equation 8 shows the final expression for the escaping radiation intensity after consolidating all aspects of consideration previously discussed. As mentioned, the backscatter fraction has been scaled by stucco volume fraction as some systems might exhibit lower concentrations of particles that would influence the predictions. Here indices n, m and i are positive, real numbers governing the number of boundary interfaces, the number of different scattering elements and the number of absorbing elements respectively. Although not explicitly mentioned up until this point, it should be made clear that mould porosity should be included among the absorbing factors with the appropriate volume fraction.

$$I = F\varepsilon_a\sigma T^4\sum_1^n(1-R_n)\sum_1^m\left(1-V_m S_{BS_m}\right)\left(1-e^{-\sum_1^i\alpha_i V_i}\right)$$

Equation 8. The final expression for escaping radiation intensity through an arbitrary solid

A closing consideration included in the final expression is the concept of view factors, F. This does not generally apply to investment casting as the mould structure is always parallel with the casting surface by the nature of its manufacture. This may be applicable in other casting processes, or when considering subsequent radiation interactions with other parts of the casting that present an angle to the emitter. If the absorbing media present an angle to the emitting surface, only a fraction of the surface area will

participate in absorption. This fraction is defined by the ratio of the product of the area and cosine of the angle between the absorbing material and the surface normal of the emitter, as shown in Equation 9 where subscripts *r* denotes the receiver (absorbing object) and *e* denotes the emitter.

$$F = \frac{q_r}{q_e} = \frac{A_r \cos(\theta_r)}{A_e \cos(\theta_e)}$$

Equation 9. The equation for the view factor affecting the extent of radiation intensity interaction between two surfaces

3. Experimental Investigation

Mathematical models of phenomena are useful tools for understanding the impacts on the final cast component. Comparing model predictions against experimental measurements is an essential development step in any theory to assess the agreement quality and accuracy. To this end, a typical mould used in producing Ni-based superalloy castings consisting of approximately nine layers was selected for assessment. The three compositionally distinct regions of the mould, defined as materials 1, 2 and 3, (Table 1) were investigated independently using a Jasco FT/IR-6200 Fourier transform infrared spectroscopy (FTIR) equipped with an integrating sphere.

Table 1. Details of the experimental mould composition

Material Identity	Layer	Composition		
		Name	Details	
Material 1	1	Cobalt Aluminate with 90 mesh Zircon sand	Chilches Microzir Flour 200M IC	$ZrSiO_2$ > 63.5% TiO_2 < 0.2% Fe_2O_3 < 0.15% Al_2O_3 <1.3% SiO_2 <33%
			Cobalt Aluminate Primecote® Plus	$CoAl_2O_4$ Binder
Material 2	2	Backup with 30/80 mesh Mullite sand	Ranco-Sil 140F Matrixol 30 MXC Excel X2 30/80 Sand	SiO_2 Binder Fibre Reinforcement -
Material 3	3-9	Backup with 16/30 mesh Mullite sand	Ranco-Sil 140F Matrixol 30 MXC Excel X2 16/30 sand	SiO_2 Binder Fibre Reinforcement -

The integrating sphere is an important FTIR attachment when measuring semi-transparent samples, as it allows the detector to remain offset from the incident source beam. A Gold reference standard was used to block the upper aperture during the baseline measurement, ensuring no light escapes. Both reflection and transmission data are required to obtain information on the absorption properties of a material. For reflection data, samples are positioned in place of the Gold standard at the top of the sphere and covered with an opaque lid to prevent the escape of light. For transmission measurements, the Gold standard remains in place while samples are placed directly in the path of the incident beam by covering the entry point at the left-hand side of the integrating sphere.

Producing samples suitable for testing was highly challenging, as the low penetrating power of the FTIR demanded correspondingly thin samples to investigate transmission. Although the production of thin films is possible, the fragility of such films makes multiple loading and unloading of samples without damage a challenge. A solution exists in the form of a transparent substrate on which to build the films. Sapphire is an ideal material for this application as it has optical transparency in the infrared region of the EM spectrum, preventing adverse impact on material transmission measurements. Circular Sapphire microscope slides with a thickness of 0.5 mm were used as the base for preparing all samples, where the diameter was selected to ensure complete coverage of the FTIR apertures. Three samples were produced on individual Sapphire slides, one for each material (1, 2 and 3) with each receiving a rainfall sanding of stucco (in line with foundry application processes). Before experimentation, all samples were fired in a muffle furnace to ensure they were representative of true production mould components. The

heating and cooling ramps were intentionally selected to be gradual to minimise the risk of cracking the films, with several pauses during the increase made for the same reason as outlined in Table 2.

Table 2. The stages of sample heating during the firing of the thin films before the FTIR assessment

Stage	Temperature range (C)	Rate (K min^{-1})
1	21 → 300	20
2	300	Hold for 5 minutes
3	300 → 600	20
4	600	Hold for 5 minutes
5	600 → 900	20
6	900	Hold for 5 minutes
7	900 → 1050	20
8	1050	Hold for 90 minutes
9	1050 → 21	20

Conducting the FTIR assessment on the samples gives reflectance and transmission results illustrated in the upper panels of Figure 1. The reflectance and transmittance results are not a single measurement but are an average from five repeat measurements. Each measurement was taken targeting a different area of the sample, ensuring subtle variations in surface finish or thickness would not negatively impact the final result. The effect of such variations does not appear to notable impact the measurement as the uncertainty bound remains tightly constrained around the mean. There is a marginally higher uncertainty in the absorbance as the uncertainty in both reflectance and transmission propagates into absorbance mathematically. Absorbance calculation is exceedingly simple, relying on energy conservation; the sum of reflectance, transmittance and absorbance must equal 100% at any wavelength.

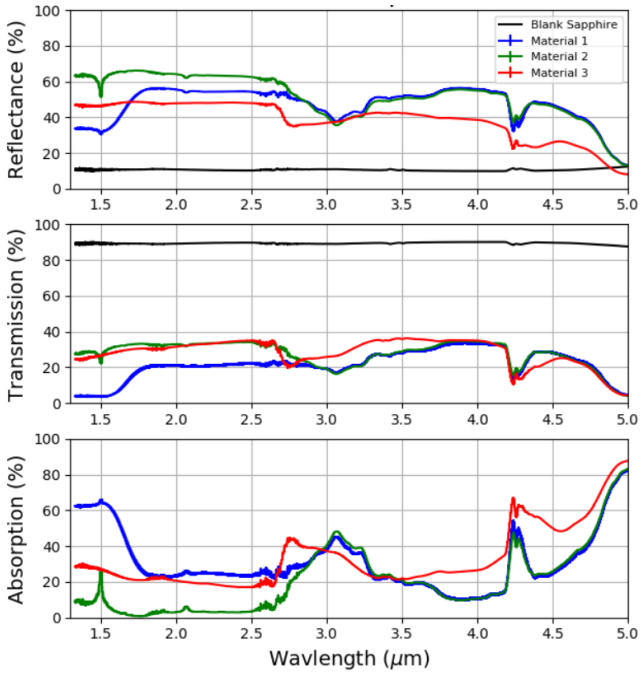

Figure 1. FTIR results for materials 1,2 and 3 showing the percent reflectance and percent transmittance alongside calculated percent absorbance. A measurement of a blank Sapphire slide (black) was taken for comparative purposes

In general, the reflectance of the samples in all cases dominates the optical properties with the greatest percentage contribution. Several troughs are present in the profile with corresponding peaks in absorbance, indicating elemental absorption bands present in the materials. Interestingly, there is a non-

zero transmittance observed in all samples across all wavelengths; an observation suggesting transparency may not be limited to defined optical windows but may operate more broadly.
Alongside the sample measurements, reflectance and transmittance measurements for a blank Sapphire slide were taken to confirm its desirable optical properties. Measurements were taken between 1.3 – 20 μm, although, above 5 μm, the Sapphire reflectance begins to rise rapidly with a corresponding decline in transmittance. This behaviour limits the useful range of experimental results to the displayed range of 1.3 – 5 μm. However, this range is sufficient. Returning to Wein's displacement law, the corresponding range of alloy surface temperatures can be estimated as 306.6 – 1956.2 °C, which comfortably covers the alloy melting, solidification interval and a significant part of subsequent cooling. The absorption coefficient can be calculated based on the measured reflectance and transmittance data using Equation 10 [8]. Knowledge of the sample thickness is needed for this calculation, which can readily be calculated based on the total sample thickness subtracting the Sapphire slide thickness. The sample thickness for materials 1, 2 and 3 were 0.44 mm, 0.47 mm and 1.42 mm respectively.

$$\alpha = \left(1 - \frac{R}{100} - \frac{T}{100}\right)\left(\frac{ln(10)}{1 \times 10^{-3} d}\right) = \frac{A}{100}\left(\frac{ln(10)}{1 \times 10^{-3} d}\right)$$

Equation 10. Method for calculation of the absorption coefficient from experimental reflectance and transmittance data with the addition of the sample thickness, d

Figure 2 shows the results of performing this calculation for the absorption coefficient in the left-hand column as a function of both wavelength and alloy surface temperature. The extinction coefficients in the right-hand panel have also been determined using the relation introduced in Equation 2. These results are considerably more relevant than the raw measurement results discussed previously as they feature thickness information; the per metre nature of these results means they are more representative of the true absorbing potential of these materials. Considering the thickness leads to enhanced absorption of material 1, which would be expected given it is the densest of the materials with a high Zircon and Cobalt concentration. As materials 2 and 3 have similar compositions, with the difference being the coarseness of the stucco, the magnitude of the absorption is similar. However, there is a considerable peak in material 2 at 3 μm which given the comparable response in material 1 is potentially a result of increased scattering of the finer stucco particles in these materials.

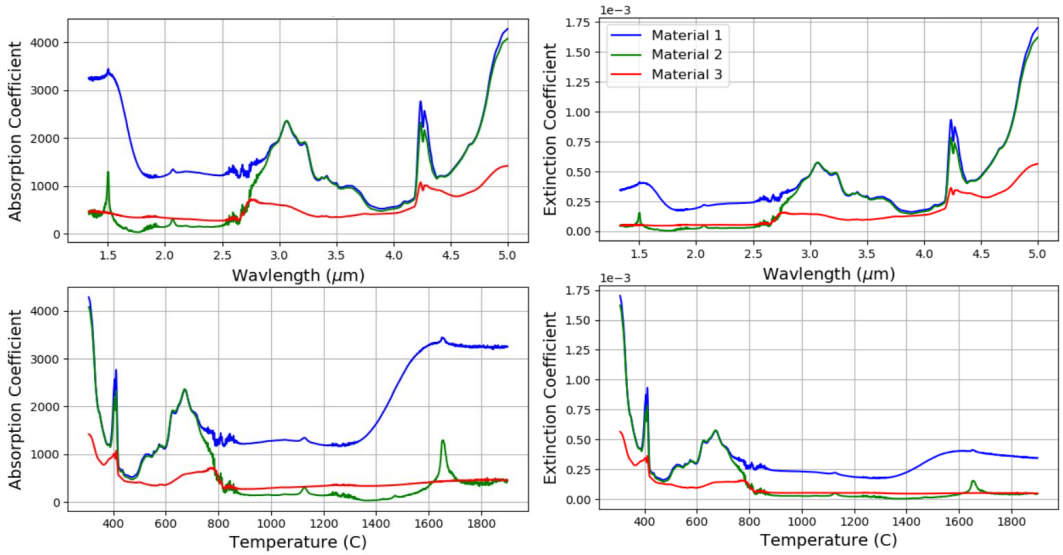

Figure 2. Results showing the calculated absorption coefficient (left column) as well as subsequently calculated extinction coefficient (right column) as a function of wavelength (top) and alloy surface temperature (bottom) for materials 1, 2 and 3

Considering the extinction coefficients as a function of temperature, the coefficient has a low value at elevated casting temperature (indicating enhanced transparency) before all materials exhibit a sudden increase in opacity around an alloy temperature of 800 C. This result is exciting as it implies significant

transparency across alloy melting, solidification and several hundred degrees of subsequent cooling. This has the potential to give rise to greater cooling than expected during a period of critical microstructural and residual stress formations that may not be accurately understood or captured by computational models of the casting process.

The final consideration is to combine the calculated extinction coefficients from FTIR analysis with the correct material thicknesses of a true production mould to assess the extent of mould transparency in a real situation. Because the absorption coefficient obtained experimentally already contains information on the boundary reflection and scattering features, the true behaviour of a production mould can be evaluated using a far simpler expression (Equation 11). This expression is related to the information discussed during the construction of the theory, but only concerns the exponential decay of initial radiation intensity. A factor of 100 has been added and the expression divided by I_0 to allow the percentage of incident radiation that will escape the mould system to be calculated.

$$\frac{I}{I_0} = 100e^{-\alpha_1 x_1 - \alpha_2 x_2 - \alpha_3 x_3} \qquad [\%]$$

Equation 11. Expression for the percentage radiation escape applied to the experimental measurements to determine real behaviour

Figure 3 shows the final comparison between the measured experimental transparency and that predicted by the model introduced in this work. Considering the experimental results initially, across the range of wavelengths presented, there are two distinct windows of transmission separated by a deep absorbance band centred ~3 μm. This is likely the result of atmospheric water [9] as experiments were not conducted in a vacuum. Both transmission peaks represent a significant amount of radiation escape with peak values of approximately 7.5 % and 4.5 %. Applying the conversion between wavelength and temperature and narrowing the range of interest to 750 – 1450 °C (because the vast majority of interesting solidification behaviour occurs across this range), it was found that only the first peak of the wavelength plot is present. It appears in the temperature-dependent plots as a mirror image due to the inverse relationship between temperature and wavelength. It is fascinating that radiation transparency is non-zero across the entire duration of mould filling, alloy solidification and initial cooling to 800 °C, a feature of such ceramic mould that is likely poorly understood within the industry. Such transparency would have the effect of steepening the cooling in the alloy in susceptible systems that potentially introduce unexpected or undesirable solidification behaviour into cast components. Moreover, this phenomenon is highly influenced by variations in mould thickness that can give rise to local enhancements or reductions in the alloy cooling rate.

The predictions from the theoretical model were generated using data from several literature sources, as detailed in Table 3. Due to materials 2 and 3 being compositionally identical and stucco size being the only dividing factor, the decision was made to amalgamate these materials into a single entity, defined as the backup region, to simplify the calculation. Elements with a ‘calculation’ source were determined during the investigation of the mould materials during previous unpublished work, which will be summarised herein. Consulting scanning electron microscope images of the mould cross-section using Fiji image analysis software [10], converting the backscatter electron image to a binary format allows identification of the percent porosity in the backup region. This method identifies a 21 % porosity where the remainder is split approximately evenly between the Silica matrix and Aluminosilicate sand. Material 1, known as the prime coat, was more complex as the volume fractions could not be determined from image analysis alone. Instead, it was estimated based on the mass of materials in the slurry, assuming the volatile binders would burn away during firing to leave a 0.075 % porosity. The fractions of Zircon and Cobalt Aluminate were estimated directly based on masses against the total mass in the slurry.

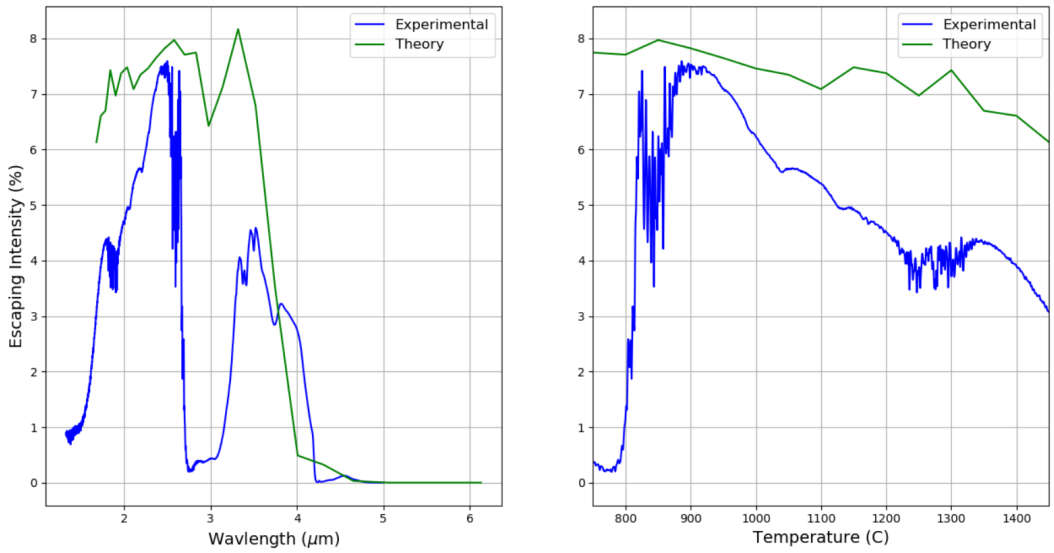

Figure 3. Comparison plots of theoretical model prediction (green) and calculation from experimental measurements (blue) as a function of wavelength (left) and temperature (right)

Estimations from the theoretical model have a reasonable agreement with the experimental measures, in which critical features such as the double peak in transmission and the gradual reduction in transmission at low wavelengths. However, the extent of these drops in transmission is underestimated. As minimal consideration of different crystallographic structures forming during sample firing was given, it is possible that increased absorption or scattering from these different structures may be responsible for this discrepancy – this will require additional investigations to confirm. In general, the theory accurately predicts the magnitude and approximate profile of transmitted radiation although further refinement will be needed to capture the nuances of radiation transparency.

Table 3. Catalogue of data sources used in the determination of theoretical model predictions

Parameter	Value	Source
Alloy emissivity	Tabular data	[11]
Refractive index (prime matrix)	1.7	[12]
Refractive index (prime stucco)	1.94	[12]
Refractive index (backup matrix)	1.44	[12]
Refractive index (backup stucco)	1.65	[12]
Extinction Coefficient (prime)	Tabular data	[13]
Extinction Coefficient (backup)	Tabular data	[14]
Extinction Coefficient (air)	Tabular data	[15]
Volume fractions (prime)	$ZrSiO_4$–91.25, $CoAl_2O_3$–8% Porosity–0.075%	Calculated
.Volume fractions (backup)	SiO_2–39.5%, Al_2O_3–39.5%, Porosity–21%	Calculated

4. Conclusions

It has been shown through an experimental assessment conducted on a representative ceramic mould that transparency to EM radiation presents a non-negligible mechanism of heat loss that will likely impact alloy cooling. Multiple solidification mechanisms will likely be impacted with magnitudes of 7.5% at its maximum that occurs at elevated alloy temperature. Applying general EM theory has shown that a representative model of semi-transparent materials, evaluated with reasonable literature data, can be successfully implemented. Although the fine details of this model require further investigation to tune the theory, the predictions correctly capture the key features and magnitude of radiation transparency. As this model is founded in physics common to all casting processes, its applicability is universal across multiple casting disciplines, requiring only input of the relevant material properties to ascertain the possible importance of IR transparency in a system.

High emissivity coating has been a point of active research for some time where complex geometry castings are concerned, but when considering semi-transparent materials, such materials only represent a partial solution. Specially designed coatings intended to absorb infrared radiation at selected wavelengths offers foundries the ability to prevent the unmonitored escape of radiation from the casting. Equally, this research offers a potential re-focus to existing efforts into high emissivity coatings by restricting identifying narrower wavelength ranges in which coatings should be effective. Should a stronger cooling trend be desirable in a specified region of a casting, high emissivity coating should consider enhancing effectiveness in regions of the spectrum where the natural transmittance of the mould is poorer.

Acknowledgements
The authors wish to thank the Engineering and Physical Sciences Research Council (EPSRC) [Grant EP/L016389/1] and TPC Components AB for funding this research.
The author would like to thank Cranfield University for providing access to the scientific equipment used in this investigation and TPC Components AB for providing the necessary materials for sample construction.
Data associated with this work is stored on the Cranfield Online Research Data repository, available to access through 10.17862/cranfield.rd.22153778.

References

[1] A. A. Keste, S. H. Gawande, and C. Sarkar, “Design optimization of precision casting for residual stress reduction,” *J. Comput. Des. Eng.*, vol. 3, no. 2, pp. 140–150, 2016.
[2] C. A. Jones *et al.*, “A verification of thermophysical properties of a porous ceramic investment casting mould using commercial computational fluid dynamics software,” *IOP Conf. Ser. Mater. Sci. Eng.*, vol. 861, 2020.
[3] R. M. Eisberg, *Fundamentals of Modern Physics*. John Wiley & Sons, 1961.
[4] X. U. Zhang, D. J. Faber, A. L. Post, T. G. van Leeuwen, and H. J. C. M. Sterenborg, “Refractive index measurement using single fiber reflectance spectroscopy,” *J. Biophotonics*, 2019.
[5] O. Boucher, *Atmospheric Aerosols*. Springer, 2015.
[6] F. Zhang and J. Li, “A note on double Henyey–Greenstein phase function,” *J. Quant. Spectrosc. Radiat. Transf.*, vol. 184, pp. 40–43, 2016.
[7] T. Binzoni, T. S. Leung, A. H. Gandjbakhche, D. Rüfenacht, and D. T. Delpy, “The use of the Henyey-Greenstein phase function in Monte Carlo simulations in biomedical optics,” *Phys. Med. Biol.*, vol. 51, no. 17, 2006.
[8] M. T. Abdullah, L. M. Raoof, M. H. Hasan, A. N. Abd, and I. M. Mohammed, “The Effect of Different Thickness on the Optical and Electrical Properties of TiO2Thin Films,” in *Journal of Physics: Conference Series*, 2021, vol. 1999.
[9] National Institute of Standards and Technology, “Water Infrared Spectrum,” *NIST Chemistry WebBook*, 1969. [Online]. Available: https://webbook.nist.gov/cgi/cbook.cgi?ID=C7732185&Type=IR-SPEC&Index=1. [Accessed: 02-Jan-2023].
[10] J. Schindelin, I. Arganda-Carreras, and E. Frise, “Fiji: an open-source platform for biological-image analysis,” *Nat. Methods*, vol. 9, no. 7, pp. 676–682, 2012.
[11] B. P. Keller, S. E. Nelson, K. L. Walton, T. K. Ghosh, R. V. Tompson, and S. K. Loyalka, “Total hemispherical emissivity of Inconel 718,” *Nucl. Eng. Des.*, vol. 287, pp. 11–18, 2015.
[12] Malvern Instruments, “Sample dispersion and refractive index guide - Mastersizer 2000.” 2007.
[13] E. D. Palik and R. Khana, “Zircon (ZrSiO4),” in *Handbook of Optical Constants of Solids III*, 1998, pp. 987–999.
[14] R. Kitamura, L. Pilon, and M. Jonasz, “Optical Constants of Silica Glass for Extreme Ultraviolet to Far Infrared at Near Room Temperature,” *Water Res.*, vol. 46, no. 33, 2007.
[15] R. W. Fenn, S. A. Clough, W. O. Gallery, R. E. Good, F. X. Kneizys, J. D. Mill, L. S. Rotherman, E. P. Shettle, F. E. Volz, “Chapter 18: Optical and Infrared Properties of the Atmosphere,” in *Handbook of Geophysics and the Space Environment*, 1985.

2023-06-18

A mathematical examination of the impact of mould transparency to infrared radiation on solidification during the investment casting process

Jones, Christopher A.

IOP Publishing

Jones CA, Jarfors AEW, Rogers E, et al., (2023) A mathematical examination of the impact of mould transparency to infrared radiation on solidification during the investment casting process. IOP Conference Series: Materials Science and Engineering, Volume 1281, Article number 012040
https://doi.org/10.1088/1757-899X/1281/1/012040